

Landau Levels and Quantum Hall Effect in Graphene Superlattices

CheolHwan Park^{1,2}, YoungWoo Son³, LiYang^{1,2}, Marvin L. Cohen^{1,2}, and Steven G. Louie^{1,2}¹Department of Physics, University of California, Berkeley, California 94720 USA²Materials Sciences Division, Lawrence Berkeley National Laboratory, Berkeley, California 94720 USA³School of Computational Sciences, Korea Institute for Advanced Study, Seoul 130-722, Korea

(Dated: February 21, 2024)

We show that, when graphene is subjected to an appropriate one-dimensional external periodic potential, additional branches of massless fermions are generated with nearly the same electron-hole crossing energy as that at the original Dirac point of graphene. Because of these new zero-energy branches, the Landau levels at charge neutrality become $4(2N + 1)$ -fold degenerate (with $N = 0, 1, 2, \dots$, tunable by the potential strength and periodicity) with the corresponding Hall conductivity σ_{xy} showing a step of size $4(2N + 1)e^2/h$. These theoretical findings are robust against variations in the details of the external potential and provide measurable signatures of the unusual electronic structure of graphene superlattices.

The physical properties of graphene [1, 2, 3] are currently among the most actively investigated topics in condensed matter physics. Graphene has the unique feature that the low-energy charge carriers are well described by the two-dimensional (2D) massless Dirac equation, used for massless neutrinos, rather than by the Schrödinger equation [2, 3]. Moreover, graphene is considered to be a promising candidate for electronics and spintronics applications [4].

It has been shown that, because of their gapless energy spectrum and chiral nature, the charge carriers in graphene are not hindered by a slowly varying electrostatic potential barrier at normal incidence [5], analogous to the Klein tunneling effect predicted in high-energy physics. Direct evidences of Klein tunneling through a single barrier in graphene [5] have been observed in recent experiments [6, 7].

Application of multiple barriers or periodic potentials, either electrostatic [8, 9, 10, 11, 12] or magnetic [13, 14, 15, 16], to graphene has been shown to modulate its electronic structure in unique ways and lead to fascinating new phenomena and possible applications. Periodic arrays of corrugations [17, 18, 19] have also been proposed as graphene superlattices (GSs).

Experimentally, different classes of GSs have been fabricated recently. Patterns with periodicity as small as 5 nm have been imprinted on graphene through electron-beam induced deposition of adsorbates [20]. Epitaxially grown graphene on the (0001) surface of ruthenium [21, 22, 23, 24, 25] and that on the (111) surface of iridium [26, 27, 28] also show superlattice patterns with 3 nm lattice period. The amplitude of the periodic potential applied to graphene in these surface systems has been estimated to be in the range of a few tenths of an electron volt [22]. Fabrication of periodically patterned gate electrodes is another possible way of making GSs with periodicity close to or larger than 20 nm.

The quantum Hall plateaus in graphene take on the unusual values of $4(1 + 1/2)e^2/h$ where 1 is a non-negative integer [29]. The factor 4 comes from the spin and val-

ley degeneracies. In bilayer graphene, the quantum Hall plateaus are at $4le^2/h$ with l a positive integer [30]. These unconventional quantum Hall effects have been experimentally verified [2, 3, 31], providing evidences for 2D massless particles in graphene and massive particles in bilayer graphene.

In this paper, we investigate the LLs and the quantum Hall effect in GSs formed by the application of a one-dimensional (1D) electrostatic periodic potential and show that they exhibit additional unusual properties. We find that, for a range of potential shapes and parameters, new branches of massless fermions are generated with electron-hole crossing energy the same as that at the original Dirac point of pristine graphene. These additional massless fermions affect the LLs qualitatively. In particular, the LLs with energy corresponding to the Fermi energy at charge neutrality (i.e., zero carrier density) become $4(2N + 1)$ -fold degenerate ($N = 0; 1; 2; \dots$), depending on the strength and the spatial period of the potential (pristine graphene corresponds to $N = 0$). Accordingly, when sweeping the carrier density from electron-like to hole-like, the quantum Hall conductivity in such a GS is predicted to show an unconventional step size of $4(2N + 1)e^2/h$ that may be tuned by adjusting the external periodic potential.

In our study, the electronic structure of the GSs is evaluated using the methods developed in Ref. 9; we evaluate the band structure of the GS numerically by solving the 2D massless Dirac equation with the external periodic potential included using a plane wave basis. Similarly, to obtain the LLs, the eigenstates of the GSs under an external perpendicular magnetic field are expanded with plane waves. We work in a Landau gauge with the vector potential depending on the position coordinate along the direction of the periodicity of the GS, and a zigzag form for the vector potential with a very large artificial periodicity (large compared to the GS periodicity) is employed to mimic a constant magnetic field near the origin in position space [32]. We have checked that the LLs are converged in energy to within less than 1% with respect

to the size of the supercell for the vector potential and the kinetic energy cutoff for the planewaves. The size of the largest supercell and that of the smallest sampling distance in real space used are 400 and 0.05 in units of a single unit cell, respectively.

Figure 1 (a) shows a GS formed by a Kronig-Penney type of electrostatic potential periodic along the x direction, with lattice parameter L and barrier width $L=2$. Remarkably, unlike that in graphene [Fig. 1 (b)], the band structure in a GS [Fig. 1 (c)] can have, depending on the potential barrier height U_0 , more than one Dirac point with $k_x = 0$ having exactly the same electron-hole crossing energy [33]. As Fig. 1 (c) shows, the number of Dirac points for this type of GSs increases by two (without considering the spin and valley degrees of freedom) whenever the potential amplitude exceeds a value of

$$U_0^N = 4N\hbar v_0 = L \quad (1)$$

with N a positive integer. The value of the potential barrier given in Eq. (1) corresponds to special GSs in which the group velocity along the k_y direction vanishes for charge carriers whose wavevector is near the original Dirac cone [e.g., the Dirac cone at the center in Fig. 1 (c)] [34, 35]. All the findings in this study apply in general to GSs made from a periodic potential which has both even and odd symmetries, like a sinusoidal type of potential. The results for GSs whose odd or even symmetry is broken are discussed in Ref. 36.

Figure 2 shows the evolution of the energy of the electronic states with $k_x = 0$ for a GS depicted in Fig. 1 for several different values of U_0 . As stated above, the group velocity along the k_y direction becomes zero near $k_y = 0$ when the barrier height is given by Eq. (1) [Figs. 2 (c) and 2 (e)]. When U_0 has a value between those specific values, the position of the additional new Dirac points move away from the $k_y = 0$ point along the k_y direction with increasing U_0 . The complex behavior of the zero-energy Dirac cones revealed by our numerical calculations cannot be derived using perturbation theory [12] because k_y is not small compared to the superlattice reciprocal lattice spacing $2\pi/L$. Moreover, the pseudospin character of these additional massless fermions [e.g., the left and the right Dirac cones (not the center one) in Fig. 1 (c)] are different from that of the original massless Dirac fermions. For example, backscattering amplitude due to a slowly varying potential within one of the new cones does not vanish [36].

A natural question arising from this peculiar behavior in the electronic structure of a GS, which is topologically different from that of pristine graphene, is how the LLs are distributed. Figure 3 shows the calculated LLs of the 1D Kronig-Penney GSs depicted in Fig. 1 for various values of U_0 [38]. When the superlattice potential modulation is moderate [Fig. 3 (b)], the spacings between neighboring LLs become smaller than those in pristine graphene [Fig. 3 (a)], owing to a reduction in the

band velocity. Once U_0 becomes larger than $4\hbar v_0 = L$ ($= 0.4$ eV for $L = 20$ nm), the zero-energy LLs (corresponding to zero carrier density) become three-fold degenerate [Fig. 3 (d)]. An important point to note is that this degeneracy is insensitive to U_0 over a range of U_0 near $6\hbar v_0 = L$ because the topology of the electron bands does not change with this variation [39, 40]. Moreover, even though the massless particles of the different Dirac cones may have different band velocities, the degeneracy of the zero-energy LLs is not affected.

The dependence of the Hall conductivity σ_{xy} on the charge carrier density n most directly reflects the degeneracy of the LLs. Figure 4 schematically shows that, depending on the superlattice potential parameters, σ_{xy} of the GSs considered has a $4(2N+1)e^2/h$ step as the density is scanned from hole-like to electron-like carriers. (We have put in the additional factor 4 coming from the spin and valley degeneracies in this discussion and in Fig. 4.) Because the degeneracy of the LLs in the 1D GSs is insensitive to a variation in U_0 , this qualitative difference in σ_{xy} of the 1D GSs from that of pristine graphene (Fig. 4) is expected to be robust, and will provide a measurable signature of the unique electronic structure of the 1D GSs.

In conclusion, we have shown that the electronic structure of 1D graphene superlattices can have additional Dirac cones at the same energy as the original cones at the K and K' points of pristine graphene. These new massless particles contribute to a $4(2N+1)$ -fold degeneracy in the zero-energy Landau levels, whose signature is reflected in a $4(2N+1)e^2/h$ Hall conductivity step where $N = 0; 1; 2; \dots$ depending on the superlattice potential parameters. This feature of the electronic structure of the 1D graphene superlattices gives rise to new properties for the quantum Hall effect. Equally importantly, these new phenomena may provide a direct way to characterize the peculiar electronic structure of these systems experimentally.

C.-H.P. thanks Dmitry Novikov and Jay Deep Sau for fruitful discussions. This work was supported by NSF Grant No. DMR-07-05941 and by the Director, Office of Science, Office of Basic Energy Sciences, Division of Materials Sciences and Engineering Division, U.S. Department of Energy under Contract No. DE-AC02-05CH11231. Y.-W.S. was supported by the KRF (KRF 2008-314-C00111) and Quantum Materials Research Center (No. R11-2008-053-01002-0) through the KOSEF funded by the MEST. Computational resources have been provided by NERSC and TeraGrid.

Note added. After submission, we became aware of a recent theoretical work [41] concerning the newly generated massless fermions reported in this manuscript, with applications to transport properties.

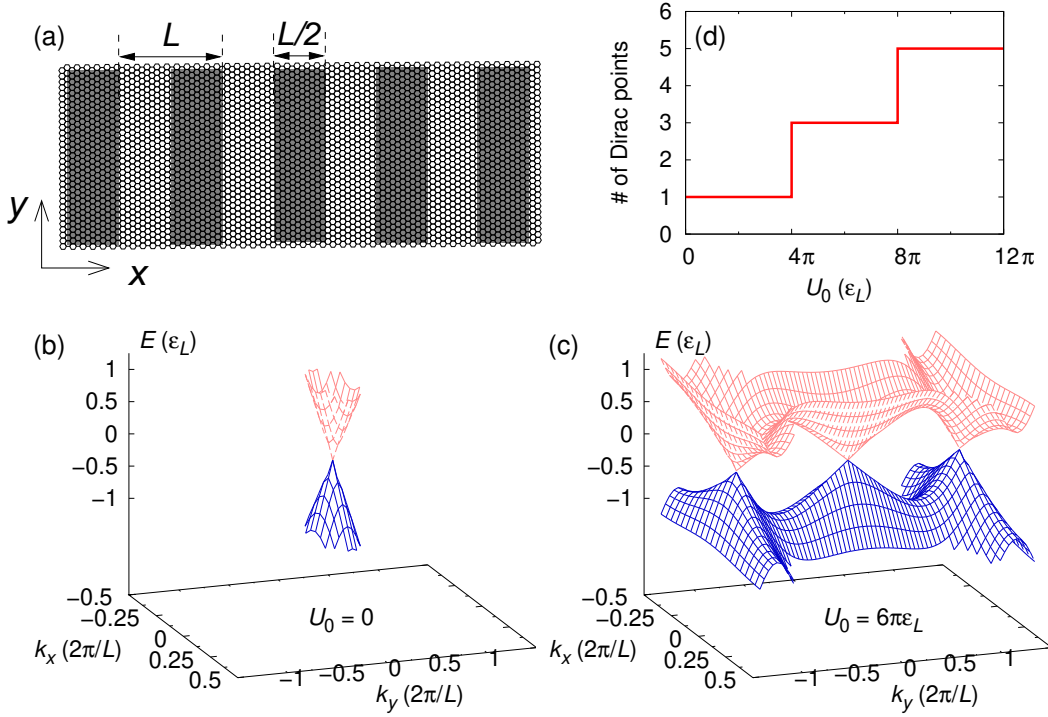


FIG. 1: (color online) (a) Schematic diagram of a Kronig-Penney type of potential applied to graphene with strength $U_0=2$ inside the gray regions and $U_0=0$ outside with lattice period L and barrier width $L/2$. (b) Electron energy in units of " ϵ_L " ($\hbar v_0=L$; for example, if $L=20$ nm, " $\epsilon_L=33$ meV) versus wavevector near the Dirac point in pristine graphene. (c) The same quantity as in (b) for a GS with $U_0=6$ " ϵ_L ". (d) Number of Dirac points (not including spin and valley degeneracies) in a GS versus U_0 .

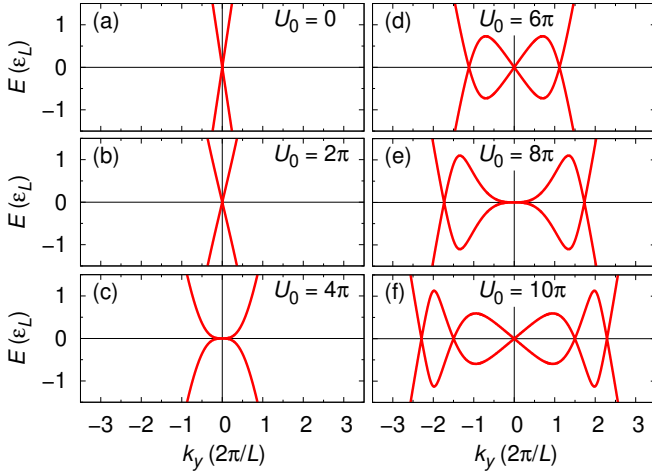


FIG. 2: (color online) Electron energy (in units of " $\epsilon_L = \hbar v_0=L$ ") versus k_y with $k_x=0$ in GSs shown in Fig. 1 for several different values of barrier height U_0 (specified in each panel in units of " ϵ_L ").

SUPPLEMENTARY INFORMATION

1. Sinusoidal superlattice

In the main manuscript, we state that the essential features in the electronic structure of graphene superlattices (GSs) revealed by considering the Kronig-Penney type of potential remain valid for GSs made with different types of periodic potentials. In this section, we support this by showing the results for GSs with sinusoidal types of external periodic potentials [Fig. 5(a)].

The function $\psi(x)$ defined by Eq. (6) in Ref. 12 for a sinusoidal type of external periodic potential $V(x) = V_0 \sin(2\pi x/L)$ is $\psi(x) = V_0 L = \hbar v_0 \cos(2\pi x/L)$. Therefore, as shown in Eqs. (9) and (15) of Ref. 12, the group velocity at the original Dirac point perpendicular to the periodic direction is given by $v_y = f_0 v_0$, where v_0 is the group velocity in pristine graphene and $f_0 = J_0(LV_0/\hbar v_0)$. Here, $J_0(x)$ is the zeroth order Bessel function of the first kind. Our calculations show that a new pair of massless Dirac points are generated whenever $f_0 = 0$, i.e., V_0 is equal to

$$V_0^N = x_{0;N} \frac{\hbar v_0}{L}; \quad (2)$$

where $x_{0;N}$ is the N -th root of $J_0(x)$ (e.g., $x_{0;1} = 2.405$,

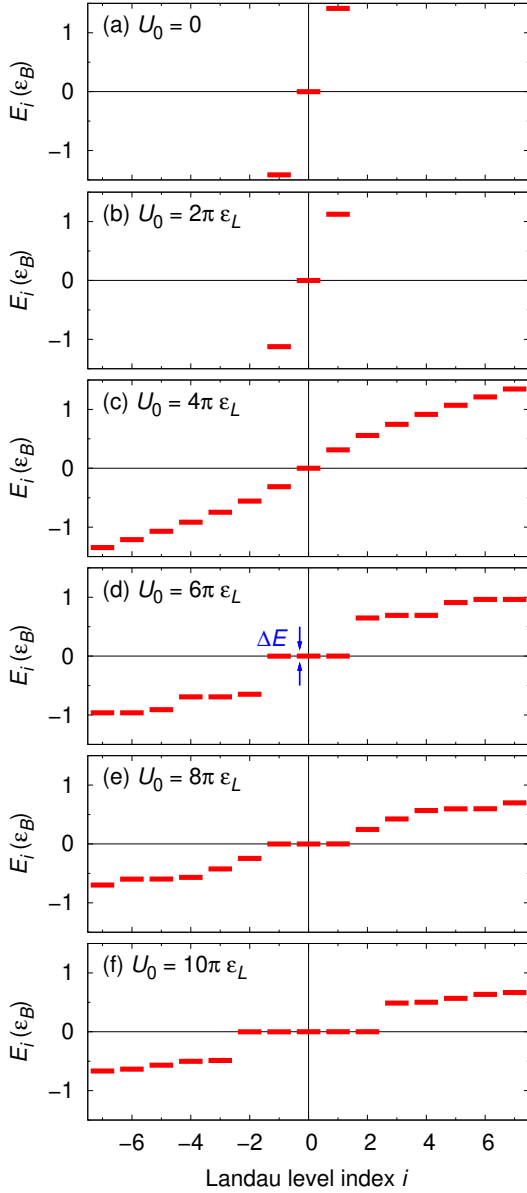


FIG. 3: (color online) Landau level energy E_i (in units of ϵ_B , $\hbar v_0 = \epsilon_B$ with $\epsilon_B = \hbar c/eB$) versus the Landau level index i ($i = 0; 1; 2; \dots$) in GSs formed with a 1D Kronig-Penney potential for several different values of barrier height U_0 , with lattice period $L = 0.5\epsilon_B$. The LLs now have a finite width ΔE (shown not to scale and exaggerated in the figure) arising from the k_y dependence of the energy of the electronic states in a perpendicular magnetic field [37]. Note the 3-fold and the 5-fold degeneracies around $E_i = 0$ in (d) and (f), respectively. (If the spin and valley degeneracies are considered, those become 12-fold and 20-fold, respectively.)

$x_{0,2} = 5.520$, etc.) [Fig. 5(b)].

Figure 5(c) shows the energy bandstructure of a sinusoidal type of GS with $V_0 = 4.0 \frac{\hbar v_0}{L}$. Because this value of V_0 is between V_0^1 and V_0^2 , a pair of new zero-energy massless Dirac cones are generated, and they clearly affect the Landau level degeneracy [Fig. 5(d)] in the same

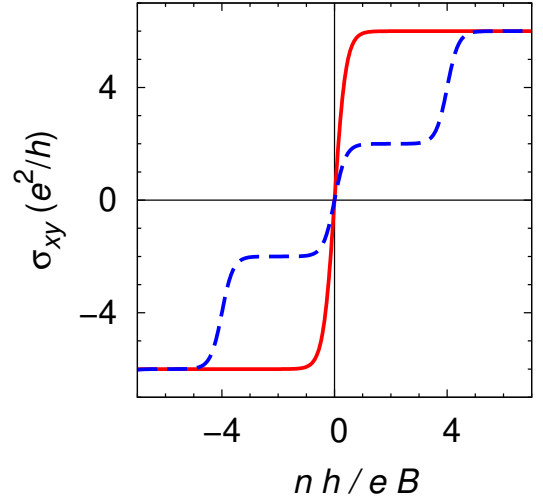


FIG. 4: (color online) Hall conductivity σ_{xy} versus carrier density (with an artificial broadening for illustration) for a 1D Kronig-Penney GS with U_0 near $6\epsilon_B$ (solid red line) is compared to that of pristine graphene (dashed blue line).

way as discussed in the main manuscript for a Kronig-Penney type of GS.

2. Effects of symmetry breaking on the newly generated massless fermions

In this section, we discuss the effect of symmetry breaking of the external periodic potential on the newly generated massless fermions. (The case of random perturbation is discussed in Ref. 42 of the main manuscript. In this section, we focus on a periodic perturbing potential that breaks the even or odd symmetry.)

Figure 6(a)-(c) repeats the results shown in the main manuscript for a Kronig-Penney type of periodic potential having both even and odd symmetries. If the odd symmetry is broken by adding an appropriate perturbation [Fig. 6(d)], new branches of massless fermions are still generated [Fig. 6(e)]. The energy at these new massless Dirac points however is different from that of the original Dirac point [Fig. 6(e)]. Even though $E_i = 0$ Landau level does not have the degeneracy coming from multiple Dirac points, some lower-index Landau levels still show this kind of degeneracy [Fig. 6(f)].

If the even symmetry is broken through a perturbing potential [Fig. 6(g)], new Dirac points are not generated [Fig. 6(h)]. However, the signature of newly generated states may still be probed with photoemission experiments or transport measurements [41].

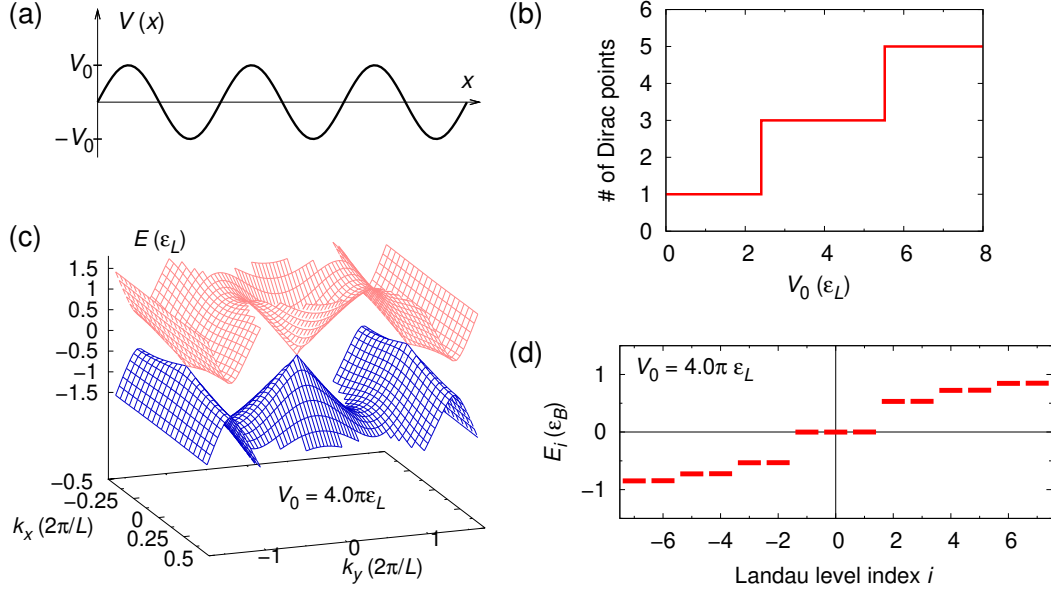


FIG. 5: (color online) (a) Schematic diagram of a sinusoidal type of potential applied to graphene with lattice period L and potential amplitude V_0 [$V(x) = V_0 \sin(2\pi x/L)$]. (b) Number of Dirac points (not including the spin and valley degeneracies) in a GS versus V_0 in units of ϵ_L ($\hbar v_0 = L$; for example, if $L = 20$ nm, $\epsilon_L = 33$ meV). (c) Electron energy versus wavevector near the original Dirac point ($k_x = k_y = 0$) for a GS with $V_0 = 4.0\pi\epsilon_L$. (d) Landau level energy E_i (in units of ϵ_B , $\hbar v_0 = l_B$ with $l_B = \hbar c/eB$) versus the Landau level index i ($i = 0; 1; 2; \dots$) in a GS formed with a sinusoidal potential with $V_0 = 4.0\pi\epsilon_L$ and $L = 0.5l_B$. Note the 3-fold degeneracy (becoming 12-fold degeneracy when the spin and valley degeneracies are considered) around $E_i = 0$.

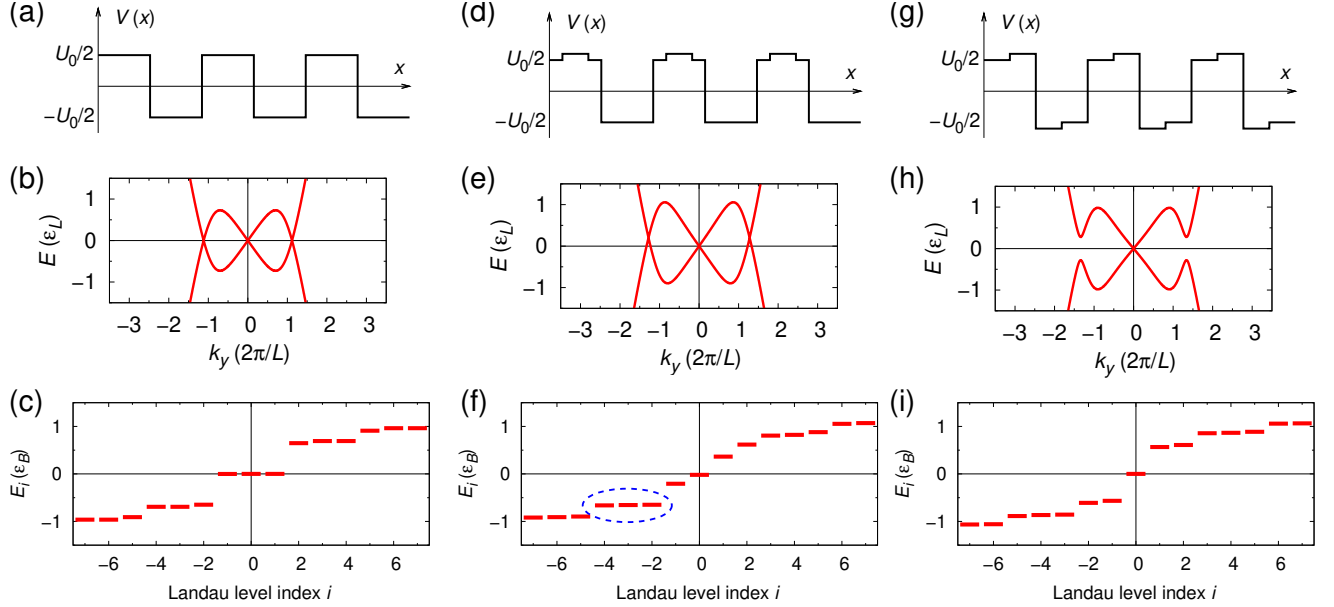


FIG. 6: (color online) (a) Kronig-Penney type of potential $V(x)$ given by $U_0/2$ for $0 < x < L/2$ and $-U_0/2$ for $L/2 < x < L$ with lattice period L . (b) Electron energy (in units of $\epsilon_L = \hbar v_0/L$) versus k_y with $k_x = 0$ in a GS formed by the periodic potential in (a) with $U_0 = 6\epsilon_L$. (c) Landau level energy E_i (in units of ϵ_B , $\hbar v_0 = l_B$ with $l_B = \hbar c/eB$) versus the Landau level index i ($i = 0; 1; 2; \dots$) in a GS depicted in (b), with lattice period $L = 0.5l_B$. (d) to (f): Same quantities as in (a) to (c) for a periodic potential $V(x)$ with a perturbation that breaks the odd symmetry. The perturbing potential $V(x)$ within one unit cell is given by +10% of the potential amplitude ($U_0/2$) for $L/8 < x < 3L/8$ and zero otherwise. Blue dashed circle in (f) shows a three-fold degenerate set of Landau levels. (g) to (i): Same quantities as in (a) to (c) for a periodic potential $V(x)$ with a perturbation that breaks the even symmetry. The perturbing potential $V(x)$ within one unit cell is given by +10% and -10% of the potential amplitude ($U_0/2$) for $L/4 < x < L/2$ and for $L/2 < x < 3L/4$, respectively, and zero otherwise.

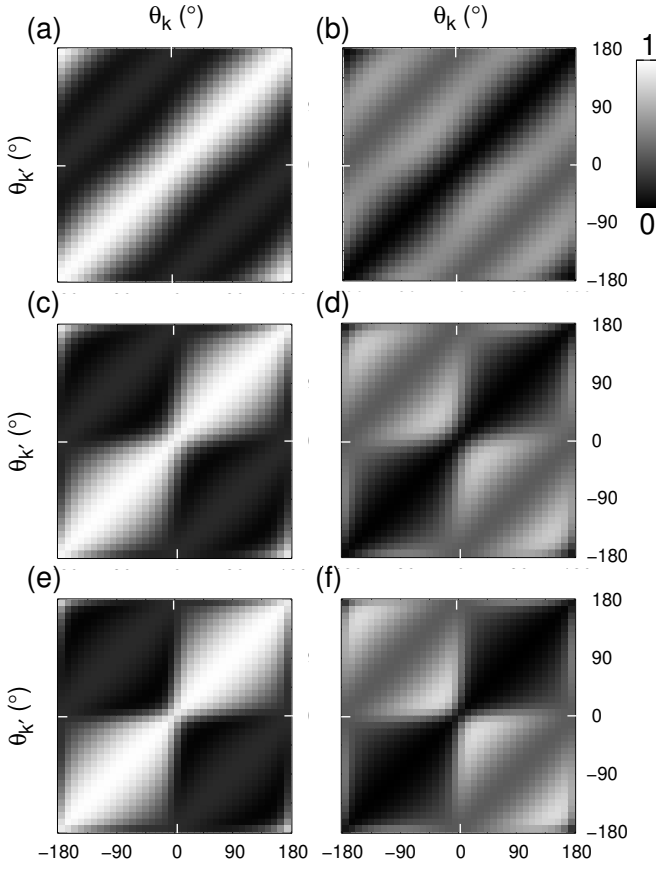


FIG. 7: (a) and (b): Calculated overlap of two quasiparticle states $\psi_{s;k}^0(\mathbf{r})$ and $\psi_{s^0;k^0}^0(\mathbf{r})$, $\int \psi_{s;k}^0(\mathbf{r}) \psi_{s^0;k^0}^0(\mathbf{r}) e^{i(k^0 - k) \cdot \mathbf{r}} d^2r$, in a GS depicted in Fig. 5(a) with $U_0 = 6 \ell_L$ versus θ_k and θ_{k^0} which are the angles between the k_x axis and wavevectors \mathbf{k} and \mathbf{k}^0 , measured from the newly-generated massless Dirac point (appearing when $U_0 = 4 \ell_L$ and moving along the k_y direction as U_0 is increased further), respectively. The overlap is shown in a gray scale (0 in black and 1 in white). The results show negligible dependence on θ_k and θ_{k^0} when they are smaller than $0.05 \pi \ell_L$ (in the figures, $\theta_k = \theta_{k^0} = 0.02 \pi \ell_L$). The two states are in the same band ($s^0 = s$) in (a) and are in different bands ($s^0 = -s$) in (b). (c) and (d), and, (e) and (f): Same quantities as in (a) and (b) for GSs with $U_0 = 8 \ell_L$ and $U_0 = 10 \ell_L$, respectively.

3. Pseudospins of new massless fermions

The pseudospin character of the newly-generated massless states are different from that of the original Dirac fermions. In order to illustrate the pseudospin character of these states, we numerically calculate the overlap $\int \psi_{s;k}^0(\mathbf{r}) \psi_{s^0;k^0}^0(\mathbf{r}) e^{i(k^0 - k) \cdot \mathbf{r}} d^2r$ of two quasiparticle states $\psi_{s;k}^0(\mathbf{r})$ and $\psi_{s^0;k^0}^0(\mathbf{r})$ in a GS having wavevectors \mathbf{k} and \mathbf{k}^0 measured from the newly-generated Dirac point (appearing when $U_0 = 4 \ell_L$ and moving along the k_y direction as U_0 is increased further). The behavior shown in Fig. 7, which corresponds to the overlap of the pseu-

dospin part of the wavefunctions, is robust if the magnitudes of \mathbf{k} and \mathbf{k}^0 are smaller than $0.05 \pi \ell_L$.

As mentioned in the main manuscript, the pseudospin character of these additional massless fermions [e.g., the left and the right Dirac cones (not the center one) in Fig. 1(c)] are different from that of the original massless Dirac fermions. Backscattering amplitude due to a slowly varying potential within one of the new cones does not vanish (Fig. 7).

Electronic address: sgbluie@berkeley.edu

- [1] C. Berger et al., *Science* 312, 1191 (2006).
- [2] K. S. Novoselov et al., *Nature* 438, 197 (2005).
- [3] Y. Zhang, J. W. Tan, H. L. Stormer, and P. Kim, *Nature* 438, 201 (2005).
- [4] X. Wu et al., *Phys. Rev. Lett.* 101, 026801 (2008).
- [5] M. I. Katsnelson, K. S. Novoselov, and A. K. Geim, *Nature Phys.* 2, 620 (2006).
- [6] N. Stander, B. Huard, and D. Goldhaber-Gordon, *Phys. Rev. Lett.* 102, 026807 (2009).
- [7] A. F. Young and P. Kim, *Nature Phys.* 5, 222 (2009).
- [8] C. Bai and X. Zhang, *Phys. Rev. B* 76, 075430 (2007).
- [9] C.-H. Park et al., *Nature Phys.* 4, 213 (2008).
- [10] M. Barbier, F. M. Peeters, P. Vasilopoulos, and J. J. Milton Pereira, *Phys. Rev. B* 77, 115446 (2008).
- [11] C.-H. Park et al., *Nano Lett.* 8, 2920 (2008).
- [12] C.-H. Park et al., *Phys. Rev. Lett.* 101, 126804 (2008).
- [13] M. R. M. Asir, P. Vasilopoulos, A. Matulis, and F. M. Peeters, *Phys. Rev. B* 77, 235443 (2008).
- [14] M. R. M. Asir, P. Vasilopoulos, and F. M. Peeters, *Phys. Rev. B* 79, 035409 (2009).
- [15] L. Dell'Anna and A. D. Martino, *Phys. Rev. B* 79, 045420 (2009).
- [16] S. Ghosh and M. Sharm, *J. Phys. Cond. Mat.* 21, 292204 (2009).
- [17] F. Guinea, M. I. Katsnelson, and M. A. H. Vozmediano, *Phys. Rev. B* 77, 075422 (2008).
- [18] T. O. Wehling, A. V. Balatsky, M. I. Katsnelson, and A. I. Lichtenstein, *Europhys. Lett.* 84, 17003 (2008).
- [19] A. Isacsson, L. M. Jonsson, J. M. Kinaret, and M. Jonsson, *Phys. Rev. B* 77, 035423 (2008).
- [20] J. C. Meyer, C. O. Girit, M. F. Crommie, and A. Zettl, *Appl. Phys. Lett.* 92, 123110 (2008).
- [21] S. Marchini, S. Gunther, and J. W. Intertlin, *Phys. Rev. B* 76, 075429 (2007).
- [22] A. L. Vazquez de Parga et al., *Phys. Rev. Lett.* 100, 056807 (2008).
- [23] P. W. Sutter, J.-I. Flege, and E. A. Sutter, *Nature Mater.* 7, 406 (2008).
- [24] D. Martoccia et al., *Phys. Rev. Lett.* 101, 126102 (2008).
- [25] Y. Pan et al., arXiv:0709.2858v1.
- [26] J. Coraux, A. T. N. D'Almeida, C. Busse, and T. Michely, *Nano Lett.* 8, 565 (2008).
- [27] A. T. N. D'Almeida et al., *New J. Phys.* 10, 043033 (2008).
- [28] I. Pletikoscic et al., *Phys. Rev. Lett.* 102, 056808 (2009).
- [29] V. P. Gusynin and S. G. Sharapov, *Phys. Rev. Lett.* 95, 146801 (2005).
- [30] E. McCann and V. I. Fal'ko, *Phys. Rev. Lett.* 96, 086805 (2006).

- [31] K. S. Novoselov et al, *Nature Phys.* 2, 177 (2006).
- [32] The zigzag form of the vector potential we used results in the perpendicular magnetic field of a uniform strength pointing along the +z direction for half the artificial periodicity and along the -z direction for the other half.
- [33] Note that these additional massless fermions with $k_x = 0$ are different from those generated at the supercell Brillouin zone boundaries discussed in Ref. 12.
- [34] The group velocity along the k_y direction is given by $v_y = v_0 \frac{\partial}{\partial k_y} \sum_{L=2}^{L=2} e^{i \phi(x)}$ where $\phi(x)$ for a Kronig-Penney type of superlattice is given by $\phi(x) = U_0 \sum_{j=1}^j \delta(x - jL)$ (see Ref. 12). When Eq. (1) is satisfied, $v_y = 0$.
- [35] The use of the Dirac equation for this problem is still valid because the new Dirac points are very close to the original Dirac point ($k_x = k_y = 0$), inside the regime where the graphene band is linear. For example, in Fig. 1(c), the new massless Dirac points appear at $k_y = \pm \frac{1}{2L} = \pm 0.034 \text{ \AA}^{-1}$ if $L = 20 \text{ nm}$.
- [36] See Supplementary Information.
- [37] R. Winkler, J. P. Kotthaus, and K. Ploog, *Phys. Rev. Lett.* 62, 1177 (1989).
- [38] When a vector potential $A(x) = Bx\hat{y}$ is used, the shift in the center of a Landau state along the x direction is proportional to k_y ; hence, in a 1D superlattice periodic along x, the external periodic potential felt by a Landau state varies with k_y , resulting in a finite Landau band width $\sim E$ (Ref. 37). However, if the level spacing between LLs is much larger than E , the signature of these LLs can be measured from experiments, as in graphene (Refs. 42 and 43). In our case, we have checked that for the zero-energy LLs plotted in Fig. 3, as long as $\ell_B > L$, E is smaller than 0.2 % of ϵ_B . Thus, in the conditions considered here, Landau bands can be considered as discrete levels, i.e., LLs.
- [39] The effect of up to 10 % disorder in the on-site potential of graphene on the LL broadening is small (Ref. 44). Since the low-energy electronic band structure of a GS can effectively be decomposed into a finite number of Dirac cones, we expect that the LLs in GSs with moderate disorder can be observed.
- [40] For a Kronig-Penney superlattice with $L = 20 \text{ nm}$ and $\ell_B = 2L$ (corresponding to $B = 0.4 \text{ T}$), the magnetic energy ϵ_B is 17 meV. In this case, temperature has to be lowered to observe the LL quantization.
- [41] L. Brey and H. A. Fertig, *Phys. Rev. Lett.* 103, 46809 (2009).
- [42] C.-H. Park and S. G. Louie, *Nano Lett.* 9, 1793 (2009).
- [43] M. G.ibertini et al, *Phys. Rev. B* 79, 241406 (2009).
- [44] W. Zhu et al, *Phys. Rev. Lett.* 102, 056803 (2009).